Two-dimensional detector software: From real detector to idealised image or two-theta scan

A. P. Hammersley [a] , S. O. Svensson [a] , M. Hanfland [a] , A. N. Fitch [a] &
D. Hausermann [a]

[a] European Synchrotron Radiation Facility , BP 220, 38043, Grenoble,
Cedex, France
Published online: 19 Aug 2006.

PLEASE SCROLL DOWN FOR ARTICLE

TWO-DIMENSIONAL DETECTOR SOFTWARE: FROM REAL DETECTOR TO IDEALISED IMAGE OR TWO-THETA SCAN

A. P. HAMMERSLEY*, S. O. SVENSSON, M. HANFLAND,
A. N. FITCH and D. HÄUSERMANN

*European Synchrotron Radiation Facility, BP 220,
38043 Grenoble Cedex, France*

Detector systems introduce distortions into acquired data. To obtain accurate angle and intensity information, it is necessary to calibrate, and apply corrections. Intensity non-linearity, spatial distortion, and non-uniformity of intensity response, are the primary considerations.

It is better to account for the distortions within scientific analysis software, but often it is more practical to correct the distortions to produce 'idealised' data.

Calibration methods and software have been developed for single crystal diffraction experiments, using both approaches. For powder diffraction experiments the additional task of converting a two-dimensional image to a one-dimensional spectrum is used to allow Rietveld analysis. This task may be combined with distortion correction to produce intensity information and error estimates.

High-pressure experiments can introduce additional complications and place new demands on software. Flexibility is needed to be able to integrate different angular regions separately, and to produce profiles as a function of angle of azimuth. Methods to cope with awkward data are described, and examples of the techniques applied to data from high pressure experiments are presented.

KEY WORDS: Data analysis, powder diffraction, detector calibration, detector distortions, area detectors, distortion correction.

INTRODUCTION

Accurate intensity determination, as a function of position or diffraction angle, from 2-D detectors depends on good detector characterisation, and on consideration of diffraction and detector geometry. In general, the following need to be considered:

Detector Characteristics: e.g., Non-linearity of intensity response, spatial distortion, non-uniformity of intensity response

Experimental Geometry: e.g., Position of the beam centre on the detector, any non-orthogonality of the detector to the direct beam

Diffraction Geometry: e.g., Polarisation effects, differential absorption

---

*To whom correspondence should be sent

Whilst considering software, it should be emphasized that data analysis is very closely linked to experimental and calibration techniques e.g., Fiducial marking is of little value if software cannot make use of the information; the converse is equally true. The primary aim is the estimation of intensities, but it is also important to estimate the standard deviation in the intensities, and care is necessary to prevent significant systematic bias.

DETECTOR DISTORTIONS

We consider the following detector distortions for calibration and correction: non-linearity of recorded value with intensity e.g., X-ray film logarithmic response; spatial distortion of recorded positions e.g., electric field distortions in a TV detector; and non-uniformity of recorded value with position e.g., unevenness in a fibre-optic taper. For image plates (IP's) there is a temperature dependent decay of the latent image with time[1,2,3]. If the scanning time is similar to the exposure time and the time between exposure and scanning, this effect may lead to an appreciable non-uniformity of intensity response. An overview of 2-D detector calibration is given in[4], and specific aspects are covered in detail in[5,6,7,8].

Recently we have developed a new technique for flood-field illumination of 2-D detectors, and for flat-field correction. It allows smooth, almost isotropic, illumination for a wide variety of X-ray wavelengths[9]. In a protein crystallagraphy test experiment we have much improved the intensity accuracy relative to previous techniques.

SINGLE CRYSTAL DIFFRACTION STUDIES

For single crystal diffraction there is experience with 2-D detector distortions[10], and software which takes into account most or all of the above considerations exists[11,12,13] e.g., MADNES. Tucker considers errors and systematic bias, owing to distortions and other aspects of the experiment[14].

However, most software has been developed for X-ray film data (or TV detectors in the cases cited), and has more recently been adapted for IP data. If a detector is used with characteristics very different from those of film or IP's, the appropriateness of the software needs to be considered. If the software is poorly adapted for a new type of detector, two different approaches may be appropriate: i. Transform the raw data to an "idealised" form, suitable for existing software; ii. Adapt the existing software to cope with the special characteristics of the detector. The first approach is more practical i.e., it is simpler and is faster to implement. The second approach should produce better results, provided that the software can be adequately adapted to the characteristics of the detector.

We are presently applying both approaches. "Idealised" data has been produced from IP data and from the ESRF X-ray Image Intensifier/CCD readout detector system. This 'idealised' data is processed with standard crystallographic software. Applied to protein crystallography, data quality similar to that obtained with widely

accepted IP systems has been obtained[4]. Spatial distortion and flat-field corrections have been incorporated into the data collection and integration program MADNES[11]. The spatial distortion correction works well, and test are being undertaken to assess the overall data quality.

POWDER DIFFRACTION USING TWO-DIMENSIONAL DETECTORS

The use of 2-D detectors for powder diffraction is relatively new and is mainly restricted to high-pressure studies. The major aspects of integrated intensity estimation are covered in[15,16,17,18,19,20]. However, detector calibration, correction, and some other aspects of the analysis deserve further attention. Software is primarily concerned with reducing 2-D data to 1-D scans; many detector distortions tend to average out and become of lesser importance. However, if different angular regions of the detector are treated separately, this averaging is reduced. Such treatment may be useful to deal with texture effects and preferred orientations.

We divide the data analysis into four main stages (cf. Sulyanov et al.[20]):

1 Calibration and determination of detector characteristics
2 Determination of experimental geometry (beam centre, tilt)
3 Application of data-reduction procedures, taking into account the detector characteristics, and the experimental geometry
4 Application of diffraction geometry related corrections

(Stages 3 and 4 may need to be performed simultaneously e.g., polarisation correction.)

Detector Calibration and Correction

Much calibration data may be obtained from scientific experimental data i.e., redundancy in the data allows parameters such as the experimental geometry to be determined. Alternatively, calibration measurements may be made separately. Each approach has advantages and disadvantages. A well designed calibration experiment may be more precise and provide more information, however, separate calibration can only be valid to the extent that the measurement is repeatable. Some calibration measurements may be combined with the experiment e.g., beam centre recording using semi-transparent beam-stops, and fiducial marking.

Masking Contaminating Features

For both beam centre and detector non-orthogonality (tilt) determination, and the rebinning of 2-D data to 1-D 2θ scans it is important to be able to mask-off contaminating features e.g., diamond Bragg reflections from the anvils in high-pressure experiments[21]. Flexible graphics are necessary for visualisation, and for ergonomic user definition of "bad data". A variety of methods are needed for removal of small circular regions (Bragg peaks), and for definition of arbitrary polygons for removal of large contaminated regions. Figure 1 shows the masking operation in
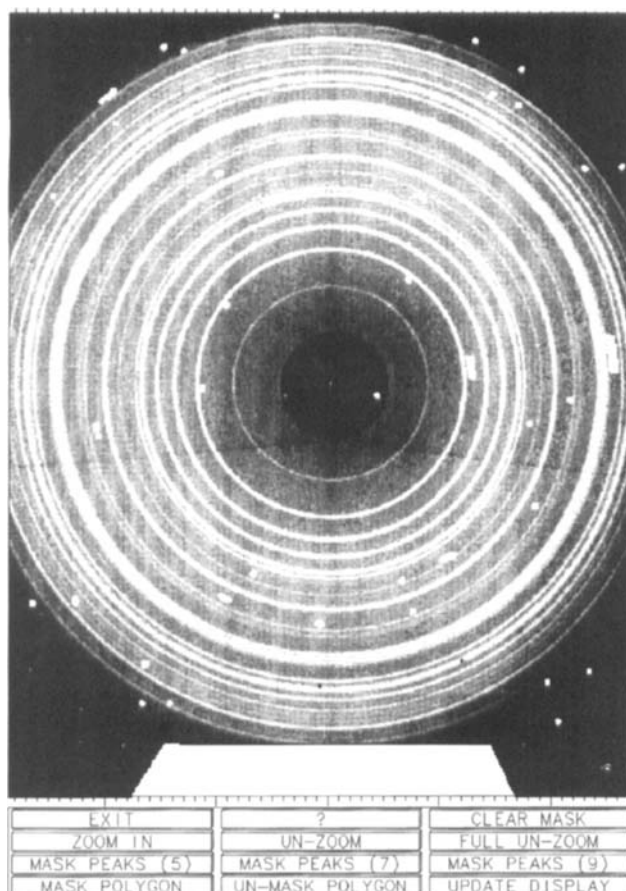
Figure 1   The "DEFINE MASK" command graphics menu from FIT2D.

FIT2D[22]. Additionally, automatic methods are desirable e.g., define all pixels with a value below a threshold as being masked-off.

Beam Centre and Detector Tilt Determination

The beam centre may be obtained with semi-transparent beam-stop, but to obtain sub-pixel accuracy the illuminated region should cover several pixels. Depending on the size of the beam, the illumination may be a record of the beam structure, or may be a radiogram of the semi-transparent region. A small beam image may be fitted by an appropriate function e.g., 2-D Gaussian, to obtain the beam centre with sub-pixel accuracy. In the case of the radiogram being defined by the semi-transparent "hole" then fitting or cross-correlation using the "hole" function may be more appropriate.

Detector tilt may be largely by careful adjustment[18]. An orthogonal detector is best, but it may not always be possible to align the detector with sufficient accuracy.

It is then necessary to calibrate the tilt from the powder rings or from fiducial marks, if available. Fiducial marks placed accurately at the corners and edges of the detector with known angles could be used to determine the tilt. This method is independent of the powder diffraction pattern and allows automatic processing.

If the powder diffraction pattern is used, it is useful to consider whether to optimise the tilt as function of ring positions[15,16,20], or as a function of position and intensity[17]. If each ring is considered to be of equal intensity with azimuth, then it is better to optimise using the intensity information. However, if rings are considered to change intensity with azimuth, it is better to consider only position. The sectoring approach of Piltz seems appropriate for obtaining a number of coordinates for each ring[17]. However, a criterion for determining the optimum number of sectors is lacking.

In general, we are interested in diffraction patterns where the intensity may change with azimuth so we consider ring position. Calculation of the centroid of rings defined over a fixed 2θ range has been used[20]. This provides a simple method, but care is needed as non-zero backgrounds can lead to bias in the results. A much better method is cross-correlation with a known peak profile function[23]. The peak centre is estimated to be the position where the cross-correlation value is a maximum. This produces better estimates of position for weak and noisy data, and can overcome the problem of sloping backgrounds for symmetric peak profiles[24,5]. Approximate functions may be used, or empirical profiles may be constructed from initial ring positions e.g., from centroid positions.

Meade developed equations for the intersection of diffraction cones with a cylindrical detector[15]. Here we consider a tilted flat detector. Since the data is in the detector coordinate system, we parameterise the diffraction geometry to produce a convenient objective fitting function in detector coordinates. We start by considering a cone in its own coordinate frame (x_c, y_c, z_c). This is tilted, and rotated to the detector coordinate frame (x_d, y_d, z_d). The origin is common for both coordinate frames (and an intermediate frame).

The cone is of opening angle 2θ and the apex is a distance d from the sample along the z_c axis. The cone is defined:

$$x_c^2 + y_c^2 = ((d - z_c) \tan 2\theta)^2 \tag{1}$$

The cone is tilted with respect to the perpendicular from the detector by an angle ϕ in a plane, we transform Eq. (1) by an angle of $-\phi$ about the y_c axis to a coordinate frame (x_t, y_t, z_t).

$$(\cos\phi x_t + \sin\phi z_t)^2 + y_t^2 = (d + \sin\phi x_t - \cos\phi z_t)^2 \tan^2 2\theta \tag{2}$$

For $z_t = 0$ (the detector plane) Eq. (2) simplifies to:

$$\cos^2\phi x_t^2 + y_t^2 = (d + \sin\phi x_t)^2 \tan^2 2\theta \tag{3}$$

The tilt plane has an angle of β with respect to the X-axis of the detector frame, so we transform Eq. (3) by an angle of $-\beta$ about the z_t axis:

$$\cos^2 \phi (\cos \beta x_d + \sin \beta y_d)^2 + (-\sin \beta x_d + \cos \beta y_d)^2$$

$$= (d + \sin \phi (\cos \beta x_d + \sin \beta y_d))^2 \tan^2 2\theta \tag{4}$$

Eq. (4) is re-arranged to calculate an effective 2θ angle ($2\theta^{\text{obs}}$) from a detector coordinate:

$$2\theta^{\text{obs}} = \arctan\left(\frac{\cos^2 \phi (\cos \beta x_d + \sin \beta y_d)^2 + (-\sin \beta x_d + \cos \beta y_d)^2}{(d + \sin \phi (\cos \beta x_d + \sin \beta y_d))^2}\right)^{1/2} \tag{5}$$

Here x_d and y_d are relative to the beam centre (x_{cen}, y_{cen}). If (x, y) is a raw detector coordinate:

$$\begin{cases} x_d = x - x_{\text{cen}} \\ y_d = y - y_{\text{cen}} \end{cases} \tag{6}$$

Eq. (5) and Eq. (6) are used for non-linear least squares optimisation of the beam centre and tilt.

With weak or contaminated data weighted fitting and rejection of out-lying coordinates may be useful. If intensity varies with azimuth it may be appropriate to weight the fit of individual ring coordinates to the estimated significance of the coordinate. This could be done by the square root of the number of counts in the background substracted peak profile, i.e., for M diffraction rings, each measured using n_j coordinates, the objective function to be minimised is:

$$S = \sum_{j=1}^{M} \sum_{i=1}^{n_j} \left(\sqrt{I_{ij} g_{ij}} (2\theta_{ij}^{\text{obs}} - 2\theta_j^{\text{model}}) \right)^2 \tag{7}$$

where: I_{ij} is the integrated profile intensity for the sector i, on ring j; g_{ij} is the detector gain for the ring coordinate i, j; $2\theta_{ij}^{\text{obs}}$ is the calculated 2θ angle based on the ring coordinate and the current model value of the beam centre and the tilt; $2\theta_j^{\text{model}}$ is the current model value of the 2θ angle of ring j (this could be a fixed value or a variable parameter).

Equation (7) assumes that positional accuracy of ring sector coordinates is proportional to integrated intensity accuracy. This may not be justified, and alternative weighting schemes may produce better results. Weighting using the intensity value at the estimated peak position may be more robust in the presence of contaminating features. e.g., if a contaminating Bragg peak shifts the estimated peak position away from the true maximum, such weighting is likely to decrease the weighting of this point in the fitting.

Fitting can be made more robust by rejecting out-lying data points, and re-fitting the reduced coordinate set. Inaccurate coordinate positions are likely to be outside the normal range of variation. A maximum limit can be defined for the number of standard deviations from the model angle that an estimated ring angle is accepted as a valid data point[25].

Radial/Angular Integration

The third stage is the conversion of a 2-D pixel image into a 1-D binned sequence or sequences. A number of different binned sequences may be required:

- "2θ scan": One sequence integrated over $360°$ (or a smaller azimuth range) as a function of diffraction angle, or radial distance from the beam centre, on an ideal orthogonal detector.
- Azimuth scan: One sequence integrated over a limited radial range as a function of azimuth.
- Multiple 2θ scans: A number of 2θ scans, each limited to a certain range of azimuth.

These different types of integration and others may be accomplished with a flexible polar coordinate transformation; where the size of the output bins may be arbitrarily varied.

The best approach to re-binning the input pixels from a 2-D Cartesian array to a 1-D or a 2-D polar coordinate array, depends on the "meaning" of the input data i.e. the characteristics of the detector system. We assume that intensity in a detector pixel has an equal and uniform probability to have come from any position within the pixel. (Note: Owing to detector point spread functions (PSF's) this will, in general, be an under-estimation of the real spread of the intensity.) It is reasonable to re-bin the intensity of input pixels proportionally to their coverage of output bins, when transformed to the output coordinate system, taking into account spatial distortion and experimental geometry. (Note: Strictly, this is not correct for a 2θ scan, since distance and angle are not completely linear, but this effect will be extremely small.) In performing such a transformation approximations may help reduce the computation required e.g., assume that spatial distortion leaves the transformed pixels with straight edges aligned to the output pixel array[6]. By totalising the sum of fractional contributions of input pixels into each output pixel, the re-binned array may be normalised. This normalised array is equivalent to a 1-D scan one pixel wide.

This re-binning process entails a loss in resolution owing to the pixellation of the output bins. This loss may be minimised by applying the spatial distortion correction together with the geometrical transformation in a single re-binning process. Resolution loss may also be reduced by "over-sampling" the output array e.g., by having twice as many output bins of half the angular or radial widths, the resolution loss is halved. Over-sampled data will be more noisy per bin, but since there will be more bins per diffraction peak, this should not be a disadvantage for Rietveld refinement. (However, R_{wp} will be larger; where $R_{wp} = \{\sum w_i \ (y_i^{obs} - y_i^{cal})^2 / \sum w_i \ (y_i^{obs})^2\}^{1/2}$). Figure 2 shows re-binned ZrO data (atmospheric pressure). One scan (triangle markers) has an angular bin size equivalent to the width of an image pixel at the beam centre. The other scan (asterisk markers) is from the same data, but with bins of half the angular size. Each data-point in both data-sets has been normalised by the number of contributing pixels, so the intensity scales coincide. The "over-sampled" data has better resolution as is seen by the improved separation of the over-lapping peaks and the better peak shapes.
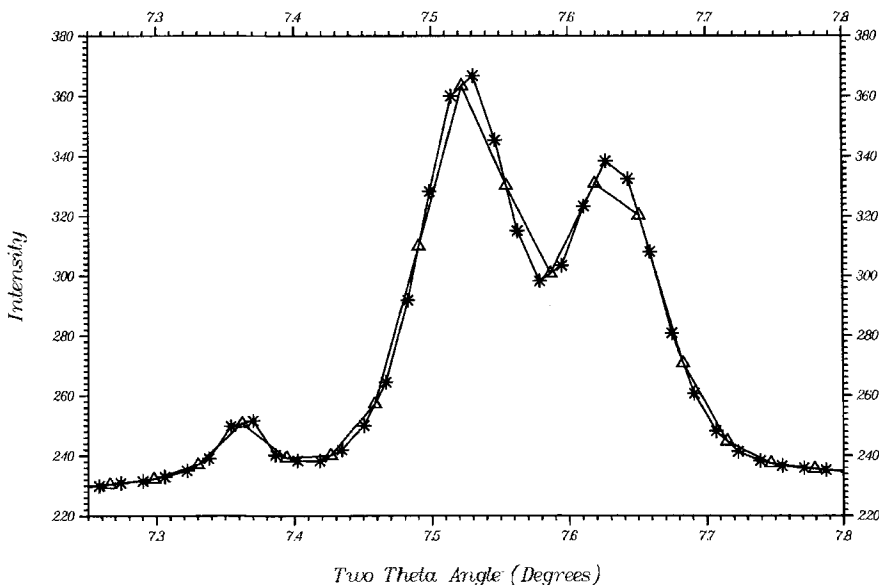
Figure 2 Demonstration of improved resolution obtained using over-sampled re-binning: the data points represented with triangle markers have been re-binned with an angular bin size equivalent to one image pixel at the beam centre; the data points represented with asterisk markers have been re-binned with angular bins of half that size.

Error Estimation

Meade shows how the second derivatives of the least squares objective function, with respect to the model parameters, may be used to calculate estimates of the errors in the beam centre, tilt, and 2θ angles, and hence d-spacings[15].

For binned intensity value error estimation, two different approaches are proposed, although neither will identify systematic bias. (The problem of avoiding systematic biases will be addressed in the next section.) If the detector gain is known, the total number of counts which have contributed to a particular bin may be used to calculate an estimate of the error for that bin. This approach is used to produce data in the "Powder Diffraction Standard" (PDS) format[26]. The PDS format expects for each bin, the normalised intensity, and a normalisation factor, such that two multiplied together produce the total number of counts measured for the bin.

An alternative is to calculate the standard deviation of an intensity value from the variation of the values which have been averaged to produce that value. The value which will be assigned to an output pixel O_i, $i = 1$ to m is the weighted average of the contributing input pixels I_j, $j = 1$ to n, where the weights w_{ij} are the fractions of the input pixels which contribute to an output pixel:

$$O_i = \frac{\sum_{j=1}^{n} w_{ij} I_j}{\sum_{j=1}^{n} w_{ij}} \qquad (8)$$

The weighted average variance is[25]:

$$\sigma_i^2 = \frac{\sum_{j=1}^{n} w_{ij}(I_j - O_i)^2}{\sum_{j=1}^{n} w_{ij}} \times \frac{N}{N-1} \tag{9}$$

The $N/(N-1)$ term accounts for the fact that the mean was itself determined from the data. Here N is best set to the sum of weights.

This may be calculated from the difference between the weighted average of the squares of the input pixels and the square of the weighted average:

$$\sigma_i^2 = \left(\frac{\sum_{j=1}^{n} w_{ij} I_j^2}{\sum_{j=1}^{n} w_{ij}} - O_i^2 \right) \times \frac{N}{N-1} \tag{10}$$

For Eq. (10) to be valid there is an important assumption: the independence of the measurements. For IP's and many other 2-D detectors the large PSF relative to the pixel size results in considerable correlation between pixels. Thus, Eq. (10) underestimates the standard deviation. A correction factor needs to be applied to account for pixel to pixel correlations. Such a correction depends on the PSF and on the distance between the pixels averaged to produce a bin value. Strictly this should be a function of 2θ angle, but for all but very small angles this will be nearly constant, so an approximate correction factor may be developed for a particular detector system.

DIFFRACTION GEOMETRY CORRECTIONS AND VERIFICATION

In addition to the aspects previously discussed, it is necessary to account for polarisation effects[27], the Lorenz correction, and absorption corrections for both the sample and the sample environment.

Intensity accuracy is best verified by calibration measurements. Through independent calibration experiments, systematic biases may be revealed, understood, and removed. The National Institute of Standards and Technology (NIST) produce calibration standards for powder diffraction, detector calibration, and other calibration purposes[28]. The reference 674a and other reference standards may be used to verify the whole system, of detector calibration, correction, integration, and scientific analysis[20,29,30]. Although care is still needed in high-pressure experiments when dealing with very small amounts of powders and very small X-ray beams.

HIGH PRESSURE EXAMPLES

Figure 3 shows the results of a Reitveld refinement of a spectrum of HgS collected at the ESRF with 0.4817Å radiation. The fine powder was contained in a Merrill-Bassett diamond-anvil cell (DAC), but the pressure was close to ambient. The cell was rocked through $+/-1°$ during a 15 mins exposure to a 25×25 μm focused undulator beam. The 2-D image was collected on a 20×25 cm IP 27.5 cm from the sample and read using a Molecular Dynamics scanner (Phosphor Imager

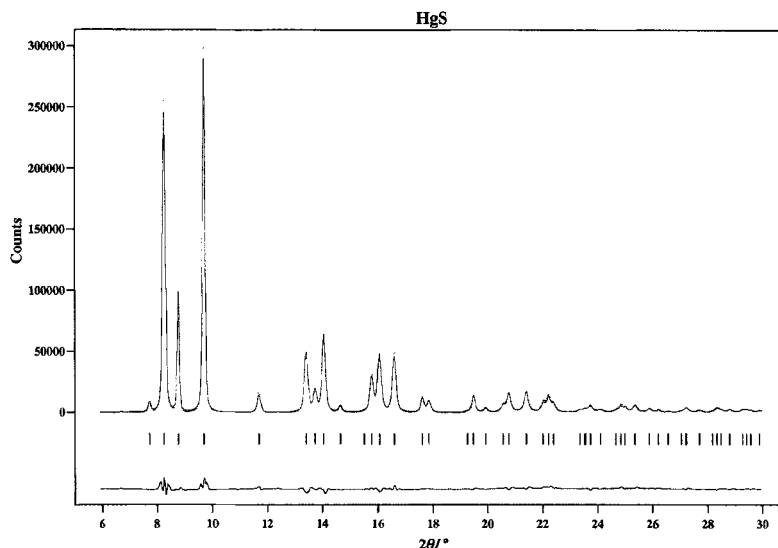244   A. P. HAMMERSLEY *et al.*

Figure 3   Output from a Reitveld refinement of an integrated 2-D image of HgS in a diamond-anvil cell.

400E, 176 μm pixels). FIT2D was used to correct and integrate the data, and MPROF was used for the Rietveld refinement, which detected the presence of a small amount of preferred orientation along the 101 direction (MPROF uses the March-Dollase model[31].) Our results agree well with those obtained by our colleagues at the SRS, Daresbury (using PLATYPUS). We obtain good R_i and R_{wp} values of 4.3 and 7.2, respectively, when taking anisotropic peak broadening into consideration.

Currently full integration of 2-D images into conventional 1-D spectra is the main form of processing when using 2-D detectors for high-pressure crystallography. However, further developments of the technique point towards the use of the 2-D information. Texture, preferred orientation and strain affect the powder ring intensities and shape, and the detailed analysis of these effects should lead to advances in the understanding of the micromechanics of high-pressure samples and, more importantly, of the detailed mechanisms of phase transitions[32].

Figure 4 shows data extracted from an image of HgTe at 12.3 GPa in a Merrill-Bassett cell to illustrate texture effects. Data was collected at the SRS, Daresbury, using a 75 μm diameter unfocused beam of 0.4654Å and the exposure was 8 hours on the 5 Tesla wiggler beam-line. The same model of IP scanner was used as that in the HgS case above, but the high-resolution mode (88 μm pixels) and a 30 cm plate-to-sample distance were used. FIT2D was used to process the image and extract the azimuthal variation of intensity for the 200, 021 and 111 reflections by integrating over 6° segments. With a suitable model, it should eventually be possible to describe completely the preferred orientation and/or texture present in the sample.

A more subtle effect is illustrated in Figure 5 which shows changes in ring radius as a function of azimuth. Data was collected from an InAs sample at 23.5 GPa in a
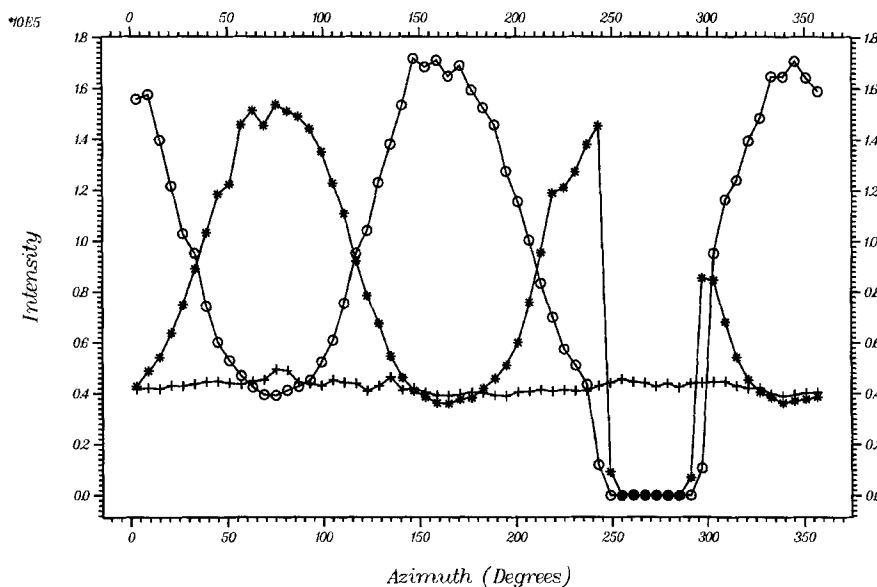
HgTe–IV at 12.3GPa (SRS)

Figure 4 The variation of the 200(∗) and 021 (o) intensities with azimuth in HgTe at 12.3 GPa. The much weaker 111 (+) intensity also shows a periodic structure when plotted on a different scale. The region of zero intensity for the two strong peaks is due to sections of the powder rings falling outside the IP.
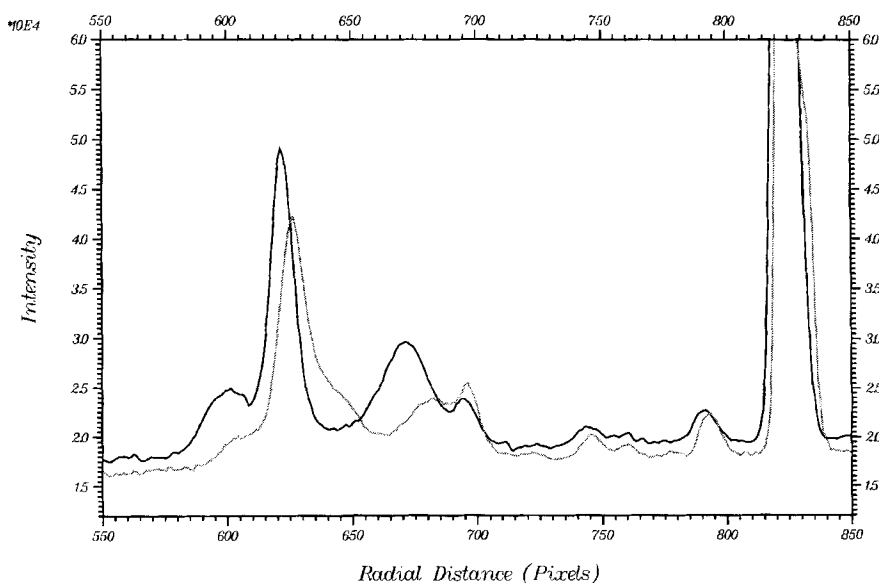
Figure 5 Peak shifts caused by strain in InAs at 23.5 GPa. These are revealed by inclining the cell with respect to the beam axis and integrating two 10° segments of the IP data at 90° to each other.

Diacell with the same experimental conditions as those for HgTe above, except for the cell orientation which was inclined at 30° with respect to the incident beam. The figure shows the same region of two 1-D spectra obtained by integrating 10° segments of the IP parallel and perpendicular to the cell inclination axis. Strain gradient(s) in the sample introduce a variation in lattice parameter for selected lines as a function of azimuth. The sample peak which is centred around radial pixel position 670 (black line) moves to around radial pixel position 685 in the profile integrated from the segment at 90° further around the azimuth (grey line). Other sample peaks also show some movement, whereas peaks from the Beryllium do not change their positions. Again suitable models should give important information on the strain distribution(s).

CONCLUSIONS

We have considered a number of aspects which need to be taken into account if accurate intensity information is to be obtained from diffraction experiments using 2-D detectors. Through the use of verification measurements, reliable integrated intensities may be obtained. We have discussed the software mainly from a theoretical or algorithmic point of view. As well as being scientifically correct and appropriate, the practical aspects of analysis software are of the utmost importance. e.g:

Applicability: The software must be able to cope with your detector data format, and must be able to run on your computer system.
Usability: The software should be easy to use. User interaction needs to be ergonomic. Documentation and on-line help information should be available to explain all user input.
Understandability: Because demands of usage vary greatly it is often required that the precise algorithms used by a program are documented.

The majority of the ideas presented here have been incorporated into the analysis program FIT2D[22]. FIT2D is still under development, but already the examples presented show its potential. FIT2D allows wide range of 2-D detector data to be treated, and is available for the most common workstations.

References

1. C. C. Shaw, J. M. Herron and D. Gur, "Signal fading, erasure, and re-scan in storage phosphor imaging", *SPIE*, **1651**, 156–162 (1992).
2. C. J. Hall, R. A. Lewis, B. Parker and J. Worgan, "2D detectors for synchrotron X-ray sources, some comparative tests", *Nucl. Instr. Meth.*, **A 310**, 215–219 (1991).

3. I. Fujii, Y. Morimoto, Y. Higuchi, N. Yasoka, C. Katayama and K. Miki, "Evaluation of X-ray Diffraction Data for Protein Crystals by Use of an Imaging Plate", *Acta Cryst.*, **B 47**, 137–144 (1991).
4. A. P. Hammersley, S. O. Svensson, A. Thompson, H. Graafsma, Å. Kvick and J. P. Moy "Calibration and correction of distortions in two-dimensional detector systems", *Rev. Sci. Instr.*, (SRI-94), March (1995).
5. A. P. Hammersley, S. O. Svensson and A. Thompson "Calibration and correction of spatial distortions in 2D detector systems", *Nucl. Instr. Meth. Section A*, **A346**, 312–321 (1994).
6. M. Stanton, W. C. Philips, Y. Li and K. Kalata "Correcting Spatial Distortions and Nonuniform Response in Area Detectors", *J. Appl. Cryst.*, **25**, 549–558 (1992).
7. D. J. Thomas "Calibrating an area-detector diffractometer: imaging geometry", *Proc. R. Soc. Lond.*, **A 425**, 129–167 (1989).
8. D. J. Thomas "Calibrating an area-detector diffractometer: integral response", *Proc. R. Soc. Lond.*, **A 428**, 181–214 (1990).
9. J. P. Moy, A. P. Hammersley, S. O. Svensson, A. Thompson, K. Brown, L. Claustre, A. Gonzalez and S. McSweeney, "A Novel Technique for Accurate Intensity Calibration of Area X-ray Detectors at Almost Arbitrary Energy", in press, *Journal of synchrotron Radiation*.
10. Z. Derewenda and J. Helliwell "Calibration Tests and Use of a Nicolet/Xentronics Imaging Proportional Chamber Mounted on a Conventional Source for Protein Crystallography", *J. Appl. Cryst.*, **22**, 123–137 (1989).
11. A. Messerschmidt and J. W. Pflugrath, "Crystal Orientation and X-ray Pattern Prediction Routines for Area-Detector Diffractometer Systems in Macromolecular Crystallography", *J. Appl. Cryst.*, **20**, 306–315 (1987).
12. W. Kabsch, "Evaluation of Single Crystal X-ray Diffraction Data from a Position Sensitive Detector", *J. Appl. Cryst.*, **21**, 916–924 (1988).
13. J. W. Campbell, M. M. Harding and B. Kariuki "Spatial-Distortion Corrections, for Laue Diffraction Patterns Recorded on Image Plates, Modelled using Polynomial Functions", *J. Appl. Cryst.*, **28**, 43–48 (1995).
14. P. A. Tucker (1990) "Errors in Macromolecular Crystallographic Data Collection with Area Detector Based Instruments", *Report DL/SCI/R28. Proc. of CCP4 Study Weekend on Accuracy and Reliability of Macromolecular Crystal Structures*, SERC Daresbury Laboratory, Warrington, England.
15. C. Meade and R. Jeanloz "High Precision Powder X-ray Diffraction Measurements at High Pressures", *Rev. Sci. Instrum.*, **61**, 2571–2580 (1990).
16. R. J. Cernik, S. M. Clark, A. M. Deacon, C. J. Hall and P. Pattison "The Development of Synchrotron X-ray Area Detectors for Studying High Pressure Phase Transitions", *Phase Transitions*, **39**, 187–198 (1992).
17. R. O. Piltz, M. I. McMahon, J. Crain, P. D. Hatton, R. J. Nelmes, R. J. Cernik and G. Bushnell-Wye "An Imaging Plate System for High-Pressure Powder Diffraction: The Data Processing Side", *Rev. Sci. Instrum.*, **63**, 700–703 (1992).
18. O. Shimomura, K. Takemura, H. Fujihisa, Y. Fujii, Y. Ohishi, T. Kikegawa, Y. Amemiya and T. Matsushita, "Application of an Imaging Plate to High-Pressure X-ray Study with a Diamond Anvil cell", *Rev. Sci. Instrum.*, **63**, 967–973 (1992).
19. J. H. Nguyen and R. Jeanloz "A Computer Program to Analyze X-ray Diffraction Films", *Rev. Sci. Instrum.*, **64**, 3456-3461 (1993).
20. S. N. Sulyanov, A. N. Popov and D. M. Kheiker "Using a Two-Dimensional Detector for X-ray Powder Diffraction", *J. Appl. Cryst.*, **27**, 934–942 (1994).
21. R. O. Piltz "PLATYPUS User Manual", Physics Department, University of Edinburgh (1993).
22. A. P. Hammersley *ESRF Internal Report*, **EXP/AH/95-01**, FIT2D V6.4 Reference Manual V1.18 (1995).
23. D. J. Thomas "The Development of a Full Profile Analysis of Single-Crystal X-ray Diffraction Data", *J. de Physique*, Supplément au No **8**, Tome **47** (1986).
24. M. Wahl *Msc. Thesis, School of Information Science and Technology, Liverpool Polytechnic* (1991).
25. P. R. Bevington and D. K. Robinson "Data Reduction and Error Analysis for the Physical Sciences (2nd Edition)", *McGraw-Hill* (1992).
26. A. D. Murry and A. Fitch, Powder Diffraction Program Library (PDPL), University College London, UK.
27. R. Kahn, R. Fourme, A. Gadet, J. Janin, C. Dumas and D. André "Macromolecular Crystallography with Synchrotron Radiation: Photographic Data Collection and Polarization correction", *J. Appl. Cryst.*, **15**, 330–337 (1982).
28. J. P. Cline "An Overview of NIST Powder Diffraction Standard Reference Materials", *Materials Science Forum*, **166–169**, 127–134 (1994).
29. J. P. Cline, A. L. Dragoo, M. Kuchinski, L. Lum and C. R. Robbins *SRM Certificate*, National Institute of Standards and Technology, Gaitherburg, MD 20899 (1989).

30. A. Kern and W. Eysel "Experimental Whole Powder pattern Intensity Calibration in X-ray Powder Diffractometry (XRPD)", *Materials Science Forum*, **166–169**, 135–140 (1994).
31. W. A. Dollase "Correction of Intensities for Preferred Orientation in Powder Diffractometry: Application of the March model", *J. Appl. Cryst.*, **19**, 267 (1986).
32. N. G. Wright "Preferred Orientation Modelling in High-Pressure Powder Diffraction applied to Structural Studies of Semi-conductors", Ph.D. thesis, The University of Edinburgh (1994).